9C-3D seismic modelling for VTI media

R. K. Sharma and R. J. Ferguson

ABSTRACT

For comparison with real seismic data, and with synthetic data derived from fully elastic numerical methods, we present a *9C-3D* numerical modelling approach that is posed in the slowness domain. The slowness domain approach has a number of advantages: $1)$ multi-pathing with no internal reflection "simpler event registration". $2)$ Parallelizable over temporal frequency. $3)$ Stable. $4)$ High frequency. $5)$ Selectable propagating mode.Implementation of our method proceeds as follows

- Define a source $(P, SV,$ and $SH)$ at the surface, and compute the plane wave transform over the time and space coordinates so that wavefield extrapolation proceeds as a set of distributed, monochromatic extrapolation steps in depth.
- Compute an anisotropic phase shift operator, and extrapolate the source spectrum φ_0 to a reflector at a new depth Δz.
- For a given receiver orientation $(V, H_1,$ and $H_2)$ at each grid point on Δz, define a rotation matrix according to the azimuth (ϕ) and dip (θ_1) between the grid point and the polarization vector of P wave source.
- Traveltimes in anisotropic media are accommodated though plane wave transformation and phase shift, and a propagation angle is produced. For each geophone component, the polarization angle is calculated from the propagation angle.
- Apply the rotation matrix to the extrapolated wavefield.
- Extract the desired component for analysis. Our numerical results demonstrate that all 9 source-receiver combinations are reliably estimate using our procedure.

INTRODUCTION

Seismic anisotropy plays an important role in Oil and Gas exploration field in order to improve the image of target horizons (Grechka, 2009). Consequently, it is less forgiving and more detrimental to our data acquisition and processing efforts to ignore the anisotropy. It has been demonstrated that wavefield propagation through anisotropic media deviates from the isotropic case (Aki and Richards, 1980) and it is composed of two parts: kinematic and dynamic. Of interest here is kinematic analysis of wave propagation in anisotropic media. The use of travel time information to infer anisotropy of subsurface and to image seismic data motivates this choice. Further, it is known that multicomponent seismic analysis is an effective technology for risk reduction in exploration and development. In exploration stage improved imaging, direct hydrocarbon and lithology indication can be offered by multicomponent measurement while development setting facilitate improved reservoir illumination and characterization by multicomponent measurements.
The importance of the anisotropy and the multicomponent seismic over the isotropy and a single component seismic motivates author to model *9C-3D* for the vertical transverse

isotropic (VTI) media. Here, VTI media is taken into account because of its simplicity in case of the anisotropic media beyond the isotropic media.

THEORY

In seeking of seismic wave interaction with anisotropic media we extrapolate wavefield first and then apply rotation matrix on this wavefield in order to obtain multicomponent data. Now, two parts: phase extrapolation of known source wavefield, and how to build rotation matrix are discussed in the following section.
Wave field extrapolation in the plain wave domain insures efficiency in terms of computational time (Sharma and Ferguson, 2009). Given a source type, the source wavefield is extrapolated from the earth surface to reflector as

$$\varphi_{\Delta z} = \varphi_0 e^{i\,\Delta z\,q\,\omega} \tag{1}$$

where φ_0 is the spectra of the source wavefield at the surface obtained via the Fast Fourier Transform (FFT)

$$(t \rightarrow \omega, x \rightarrow p_1\,\omega, y \rightarrow p_2\,\omega)$$

of the source wavefield. Vertical slowness, q is dependent on horizontal slownesses p_1 and p_2 and seismic velocity through the scalar wave-equation. In anisotropic media, q depends on a set of elastic coefficients - α_0, β_0, δ, ϵ, and γ for transversely isotropic (TI) media. Source wavefield $\varphi_{\Delta z}$ is the wavefield at depth Δz after extrapolation, and q is the vertical slowness and is known for different seismic wave modes in anisotropic media (Ferguson and Margrave, 2008).

After extrapolation, the source wavefield resides on the reflecting plane. Together, the polarization directions of P-, SV-, and SH-waves (compression, vertical shear, and horizontal shear respectively) characterize a 3 dimensional co-ordinate system defined here as the survey co-ordinate system, while the recording coordinate system is characterized by the three component directions of a $3C$ geophone.

To model the arrival of a $3C$ wave, we rotate the co-ordinate system from the survey co-ordinate to the recording co-ordinate system to register the source energy on the vertical, in-line, and cross-line components. With the basic method of a co-ordinate system transformation (Neufeld and Clayton, 2000), we transform the survey coordinate system into the recording system by rotation θ_1 degrees about the x axis followed by a rotation ϕ degrees about the z axis.

The polarization angle (θ_1) is the angle that polarization vector of the incident compressional wave make with the vertical component of $3C$ geophone. From the basic knowledge of wave propagation through the anisotropic media it has been demonstrated that polarization direction of compression wave deviates from the propagation direction but can be computed for given propagation angle (Slawinski, 2003). Now to compute the polarization angle(θ_1), first the propagation angle(θ) is computed. Angle θ is the angle that the slowness vector of an incident plane wave makes with the vertical component of a $3C$ geophone and can be computed as described below. These angles (θ, ϕ) are defined pictorially in Figure

1.
A hypothetical geophone indicated by three orthogonal blue lines is aligned with spacial

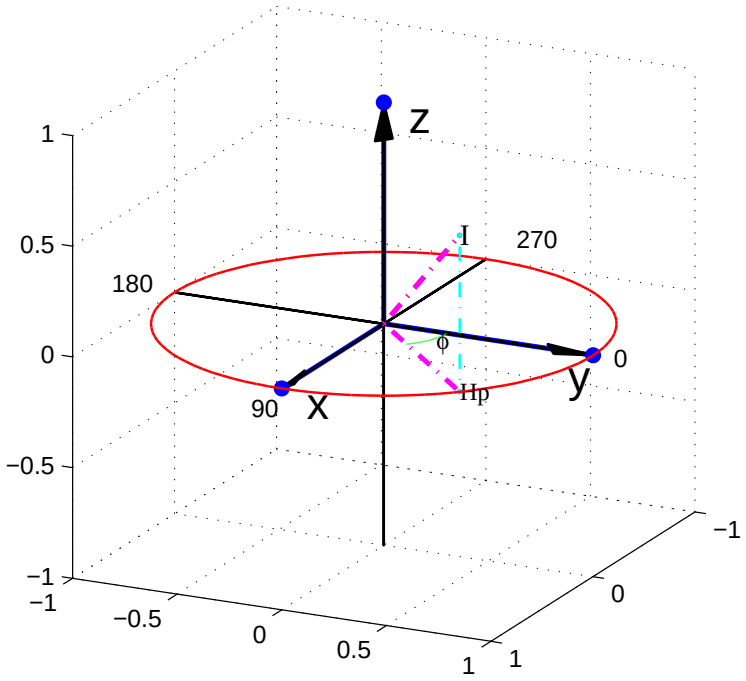

FIG. 1: A hypothetical $3C$ geophone at a grid point . "I" represents the normal to an incident plane wave and azimuth is measured relative to y axis. Azimuth ϕ indicates the in-line direction and the cross-line direction is characterized by $90°$.

axes x, y, and z. The normal to an incident plane wave is indicated by symbol "I", and the horizontal projection of "I" is indicated by H_p. Azimuth ϕ is the angle which the horizontal component y makes with H_p and indicated on this figure. The propagation angle θ is the angle between the vertical component z and "I".

The slowness vector $\hat{\mathbf{p}}$ characterizes the direction of the incident wavefield according to (Ferguson and Margrave, 2008),

$$\hat{\mathbf{p}} = \frac{p_1\,\hat{\mathbf{i}} + p_2\,\hat{\mathbf{j}} + p_3\,\hat{\mathbf{k}}}{\sqrt{p_1^2 + p_2^2 + q^2}}, \tag{2}$$

where p_1, p_2 and q are the horizontal components and vertical component of $\hat{\mathbf{p}}$ respectively. The unit normal associated with a $3C$ geophone at a grid location is

$$\hat{\mathbf{a}} = \sin\theta_a\,\cos\phi_a\,\hat{\mathbf{i}} + \sin\theta_a\,\sin\phi_a\,\hat{\mathbf{j}} + \cos\theta_a\,\hat{\mathbf{k}}, \tag{3}$$

where θ_a and ϕ_a are the dip and azimuth of the normal to the interface respectively.

The angle θ between $\hat{\mathbf{p}}$ and $\hat{\mathbf{a}}$ is then computed by cross product according to (Ferguson and Margrave, 2008)

$$\sin\theta = \left|\hat{\mathbf{p}} \times \hat{\mathbf{a}}\right|, \tag{4}$$

where $\times$ indicates cross product. Note, though we restrict our discussion here to horizontal interfaces $\left(\hat{\mathbf{a}} = \hat{\mathbf{k}}\right)$ for simplicity, we anticipate implementation of dipping interfaces as an extension to this approach.

Propagation angle θ, once computed, is used to calculate the polarization angle in terms of elastic coefficients (Slawinski, 2003). We develop a relationship between these two angles in terms of Thomson parameters (Thomsen, 1986) according to

$$\theta_1 = \tan^{-1} \frac{\left(\alpha^2(\theta) - \beta_0^2 \sin^2\theta - \alpha_0^2 \cos^2\theta\right)}{\sqrt{\left[\alpha_0^2 - \beta_0^2\right]\left[\alpha_0^2\left[2\,\delta + 1\right] - \beta_0^2\right]}\sin\theta\,\cos\theta}, \tag{5}$$

where θ_1 is the polarization angle of a P-wave where $\alpha(\theta)$ is P-wave velocity, and the polarization angle of a SV-wave when $\alpha(\theta)$ is shear wave velocity. Propagation angle θ is computed from equation 4. P-wave polarization angle can be computed from known polarization angle of SV-wave (θ_{SV}) by subtracting 90 to (θ_{SV}) (Tsvankin, 2001). Now, given θ_1 and a known source, effective $3C$ recording D_{θ_1} is computed

$$D_{\theta_1} = \begin{bmatrix} 1 & 0 & 0 \\ 0 & \cos\theta_1 & \sin\theta_1 \\ 0 & -\sin\theta_1 & \cos\theta_1 \end{bmatrix} W, \tag{6}$$

where W describes the known source type. Generally, a $3C$ source wavefield is written in matrix form as (Ferguson, 2009)

$$W = \begin{bmatrix} S_1 \\ S_2 \\ P \end{bmatrix}, \tag{7}$$

where S_1, S_2 and P are the cross-line, in-line and vertical components of the source respectively. A vertical source wavefield, for example, is written

$$W = \begin{bmatrix} 0 \\ 0 \\ P \end{bmatrix}. \tag{8}$$

Figure 2 depicts four $3C$ geophones positioned at grid points 200 m below a source position. 1, 2, 3 and 4 describe the four quadrant of a circle whose periphery trace the azimuth from 0 to 360° and has the in-line and the cross-line directions as horizontal and vertical axis. Rotation θ_1 degrees about the x axis (H_1) is anti-clockwise for geophones to the left of the source and clockwise for geophones to the right. So, we adopt the convention of a positive angle for anti-clockwise rotation and negative for clockwise rotation (Neufeld and Clayton, 2000).

Azimuth ϕ is the angle between one of the horizontal geophone components and the plane made with the source, and it is calculated from the input parameters of a plane wave. Following rotation θ_1 degrees about the x axis, the source waveform is rotated ϕ degrees about the vertical axis. A rotation ϕ about the vertical axis is computed and is written as

$$D_{\phi} = \begin{bmatrix} \cos\phi & \sin\phi & 0 \\ -\sin\phi & \cos\phi & 0 \\ 0 & 0 & 1 \end{bmatrix} W, \tag{9}$$

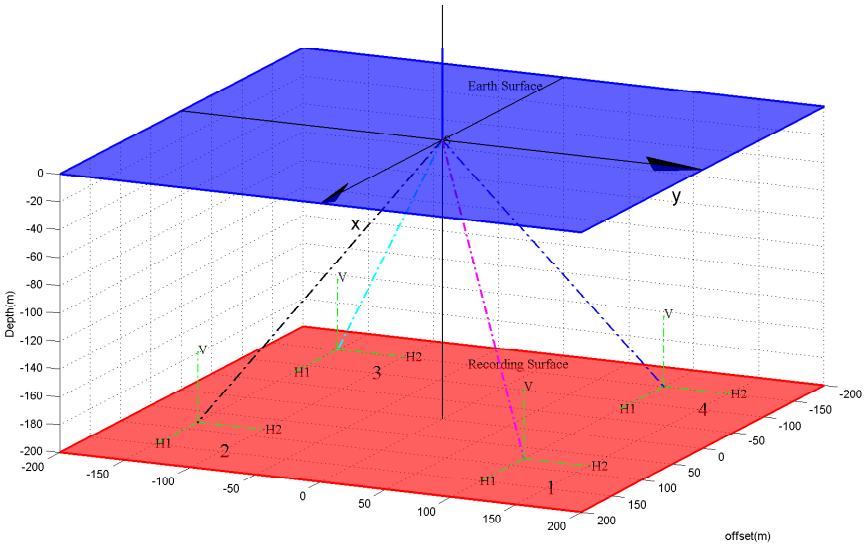

FIG. 2: Schematic representation of considered model and positioning of $3C$ geophones at reflecting surface. 1, 2, 3 and 4 describe the four quadrant of a circle whose periphery trace the azimuth from 0 to 360° and has y and x axis as horizontal and vertical axis, respectively.

As a single operation, rotation through θ_1 and ϕ is computed as

$$D = \begin{bmatrix} \cos\phi & \sin\phi\,\cos\theta_1 & \sin\theta_1\,\sin\phi \\ -\sin\phi & \cos\phi\,\cos\theta_1 & \cos\phi\,\sin\theta_1 \\ 0 & -\sin\theta_1 & \cos\theta_1 \end{bmatrix} W, \tag{10}$$

where D is the source wavefield rotated into the orientation of the $3C$ geophone. Normally it is written as (Ferguson, 2009)

$$D = \begin{bmatrix} H_1 \\ H_2 \\ V \end{bmatrix}, \tag{11}$$

where H_1, H_2, and V are the cross-line, in-line and vertical components of the vector wavefield respectively.

EXAMPLES

Since up to 75% of oil and gas producing sedimentary basins worldwide are comprised of shales and it is a major contributor to observed seismic anisotropy, a numerical model of a 700 m thick vertical transverse isotropic (VTI) medium (shale) is taken into account here. The anisotropic parameters of this shale in Thomson (Thomsen, 1986) parameters are α_0=3048 m/s, β_0 =1490 m/s, ϵ=0.255, δ=-0.27, and γ=0.480. Now a known impulsive source is extrapolated through the medium using equation1 in the plane wave domain and transformed back into the space and time domain at the interface. Further, the components of the recorded wavefield on $3C$ geophones have been sliced through the inline direction and at any given time. The red dashed line highlighted in the circle at the top right corner of Figure 3 c indicates the direction along which a vertical slice through the modelled data is taken. The in-line and cross-line directions are indicated by magenta and blue colour, respectively.

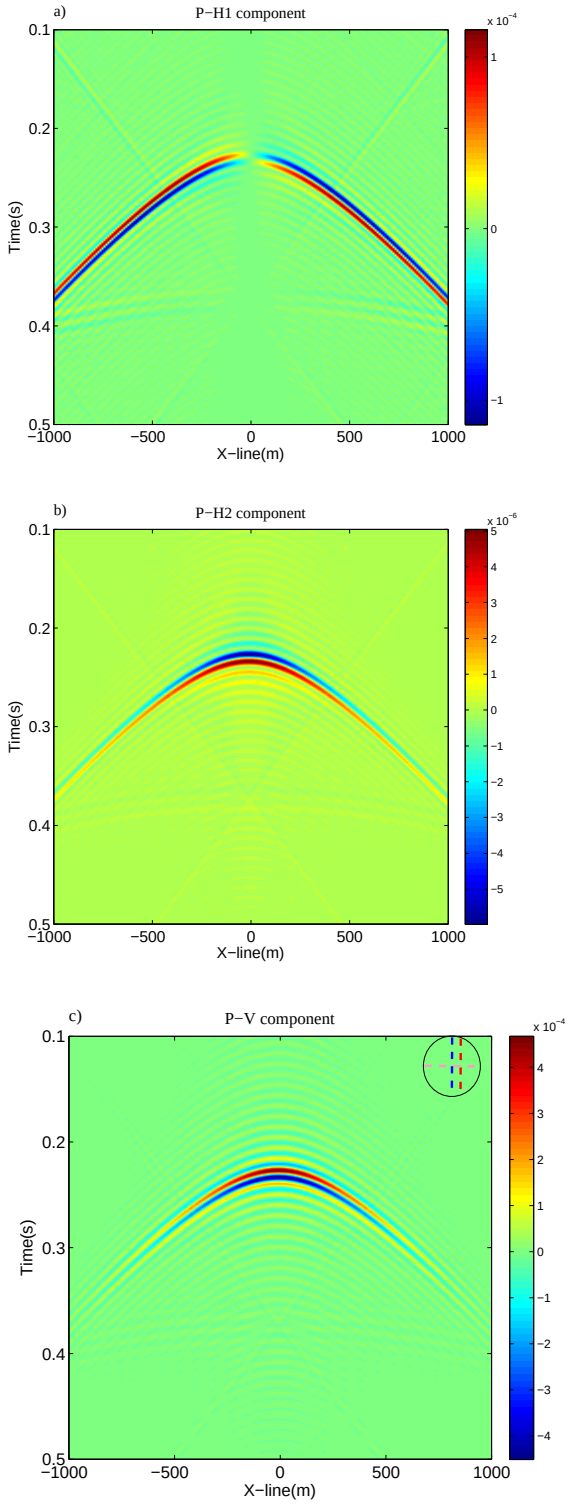

FIG. 3: (a) Registered energy versus offset (REVO) analysis of P-wave on H_1 component illustrate that H_1 component is more favourable for energy registration as offset increases. Polarity reversal appear on the either side of zero offset. (b) (REVO) analysis of P-wave on H_2 component illustrate that H_2 component is more favourable for energy registration near to zero offset. Polarity remains stationary on the either side of zero offset. (c) Recorded P-wave energy on vertical component demonstrate that energy registration on vertical component decreases with offset.

Figure 3a shows a cross-line slice of the recorded P-wave energy on H_1 component obtained through the procedure outlined above and can be represented as registered energy versus offset (REVO). REVO analysis reveals that energy registration increases with offset and polarity reversal occur on the either side of zero offset in behalf of different orientation of H_1 components with respect to source on either side. The circle in the top right corner of Figure 3c is the plan view of a recording surface where the source location is in the centre at the origin. REVO analysis of the recorded P-wave energy on H_2 component is shown in Figure 3b. It indicates that energy registration decreases with offset and polarity follow the stationary behaviour on the either side of zero offset due to same orientation of H_2 components with respect to the source on the either side. Figure 3c shows the REVO of P-wave energy on the vertical component and energy registration decreases with offset. Since the propagation angle increases with offset, it enforces the polarization angle to be increase towards H_1 component along the direction in which the slice of recorded data is taken. Thus, it makes H_1 component more favourable for energy registration at large offset and endorses the obtained REVO analysis.

Figure 4a, b and c indicate the time slices of the recorded P-wave energy on H_1, H_2 and V component ,respectively, and reveal the variation of recorded energy versus azimuth (REVA). The obtained circle in x-y plane manifests azimuthal isotropy of the medium as expected. It shows the efficacy of the proposed extrapolation method. Figure 4a demonstrates that no energy is registered on H_1 component in the in-line direction as expected. Energy registration increases as azimuth increases from 0 to 90 degree. Polarity reversal occur on the either side of a line that bisects the obtained circle along in-line direction. Since H_1 components of $3C$ geophones of quadrant 1, 2 or 3, 4 (shown in Figure 2) contain the same orientation with respect to the source, they respond to the incident wave field in the same manner. While, H_1 components of quadrant 1, 4 or 2, 3 possess antipode orientation with respect to the source and respond in a opposite way to the incident wavefield and make it possible to endorse the obtained polarity reversal behaviour. REVA analysis of the recorded P wave energy on H2 component (shown in Figure 4b) indicates that the recorded energy decreases as azimuth increases from the in-line direction to the cross-line direction. No energy is registered on H_2 component in the cross-line direction in this case as H_1 component is more favourable. Polarity on the H_2 flips from on either side of a line that bisects the obtained circle along the cross-line direction. The H_2 components of $3C$ geophones of the quadrant 1, 4 or 2, 3 respond to the incident wavefield in the similar way in behalf of the same orientation of the components with respect to the source. At the same time, the H_2 components of $3C$ geophones of the quadrant 1, 2 or 3, 4 have the opposite orientation with respect to the source and respond to the incident wavefield in a reversal manner. Figure 4c shows the variation of the recorded P wave energy with azimuth on the vertical component. It demonstrates that the recorded P-wave energy on the vertical component follow the stationary amplitude behaviour and polarity. Since, at a given time the orientation of the vertical component with respect to the incident wavefield remains constant with azimuth,thus, it reinforces the obtained REVA behaviour.

REVO analysis of the recorded SV-wave energy on H_1, H_2 and the vertical components are shown in Figure 5a, b and c, respectively. This slice demonstrates an interesting property possessed by SV-waves generated by an SV-source. For anisotropic media, SV-waves triplicate (exhibit three arrivals) when the thickness of the anisotropic medium is signifi-

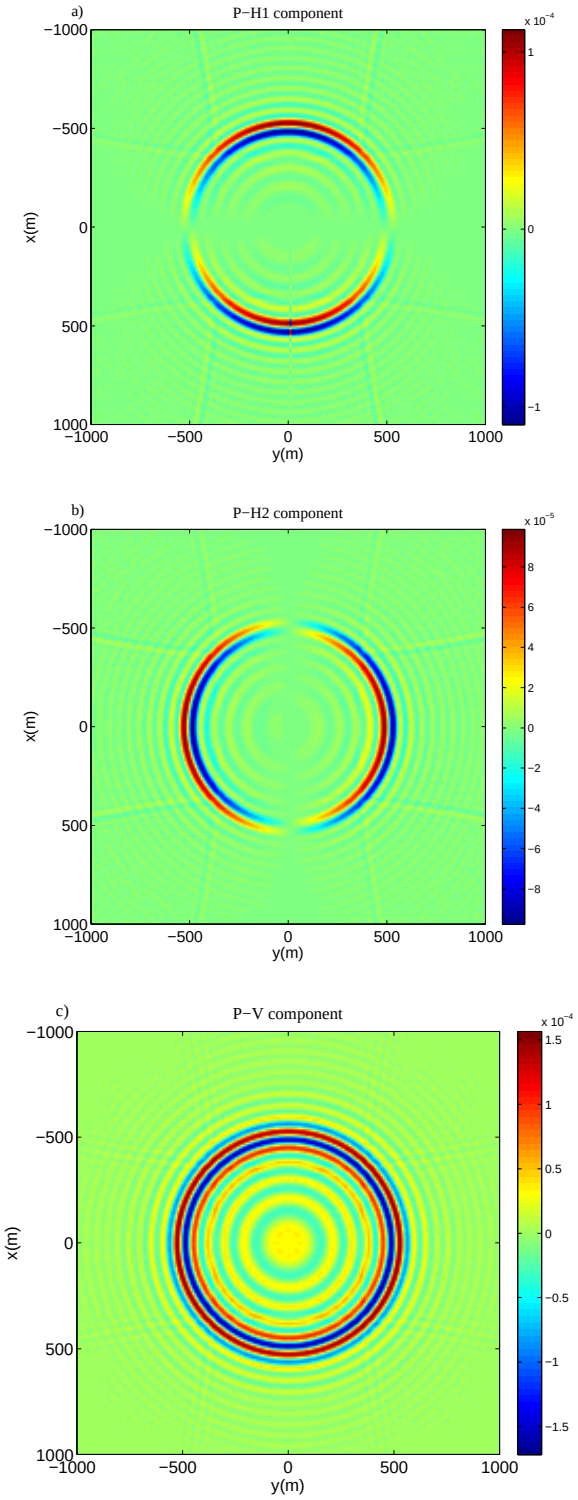

FIG. 4: (a) Registered energy versus azimuth(REVA) analysis of P-wave at H_1 component indicates that energy registration increases as azimuth increases from 0 to 90. Polarity reversal occur on the either side of a line that bisects the circle along in-line direction. (b) REVA analysis of P-wave at H_2 component indicates that energy registration decreases as azimuth increases from 0 to 90. Polarity reversal occur on the either side of a line that bisects the circle along cross-line direction. (c) REVA analysis of P-wave on vertical component reveal the variation of recorded energy and polarity with azimuth.

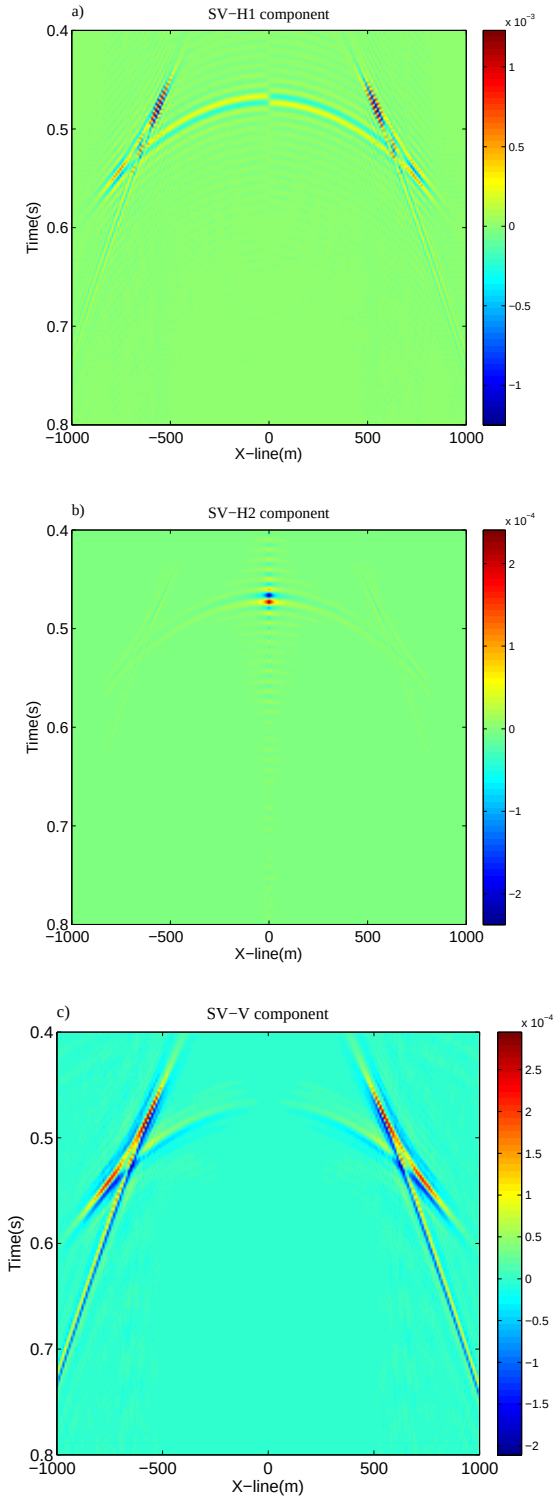

FIG. 5: (a) REVO of SV-wave on H_1 component. The Triplication phenomena occurs in this case. Registered energy decreases with offset. (b) REVO analysis of SV-wave on H_2 component demonstrate that a minuscule amount of energy is registered on H_2 component. (c) REVO analysis of SV-wave on V component indicates that a registered energy increases with offset. Polarity reversal does not occur on the either side of zero offset.

cant (Ferguson and Sen, 2004), and this is strongly apparent on V and H_1 in Figure 5. It is demonstrated by Figure 5a that energy registration on H_1 component decreases with offset and polarity reversal is also occurred on the either side of zero offset. Figure 5c shows that vertical component is more favourable for energy registration at large offset. As offset increases, the P-wave polarization angle increases with vertical. Thus, the orientation of the polarization angle of SV-wave, normal to the P-wave polarization angle, increases in the direction of the vertical component and assign it as favourable component for energy registration at large offset.

To verify the triplication phenomenon another approach described by Ferguson (Ferguson and Sen, 2004) is delineated now. According to this approach wave field extrapolation can be done using an estimate $\tilde{q}$ of true vertical slowness q and an estimate of true depth as

$$\varphi_{\Delta z} = \varphi_0 e^{-i\Delta\tilde{z}\tilde{q}\omega}. \tag{12}$$

These estimated parameters are related to the travel time error parameter, $\Delta\tau$, via

$$\Delta\tau_{sv}(p) = 2[zq(p) - \tilde{z}\tilde{q}]. \tag{13}$$

From the above equation, follows

$$-\tilde{z}\tilde{q} = \frac{\Delta\tau_{sv}(p) - 2zq(p)}{2}, \tag{14}$$

where $\Delta\tau_{sv}$ can be defined in terms of the known vertical slowness and its derivatives with respect to Thomson's parameters. Figure 6a shows the in-line slice of the extrapolated wavefield obtained by following the supporting approach and it is the facsimile of the Figure 6b. Thus, the authentication of the triplication phenomena is demonstrated. Figure 7 a,

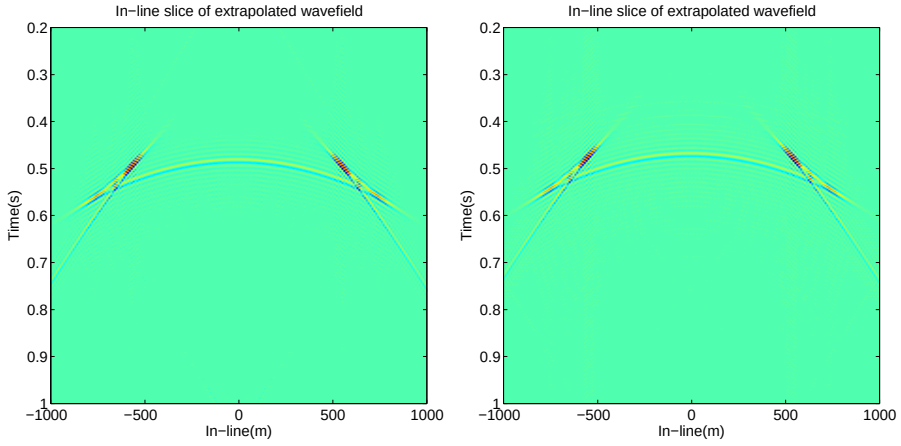

(a) (b)

FIG. 6: (a) In-line slice of the extrapolated SV wavefield by following the supportive approach and it is replica of that obtained by author and shown in (b) part. It shows the authentication of the triplication phenomena.

b and c reveal the variations of the registered SV-wave energy with azimuth on H_1, H_2 and

the vertical components, respectively. More than one concentric circle is the counterpart of triplication here. Figure 7a indicates that no energy is registered in the in-line direction as expected and the registration increases as azimuth increases. Further, polarity reversal occurs on the either side of a line that bisects the obtained circle along the in-line direction due to the different orientation of $3C$ geophones of the concerned quadrant with respect to the source. Energy registration on H_2 component decreases with azimuth and no energy is recorded on H_2 component in the cross-line direction as shown in Figure 7b. Again the polarity reversal occurs on the either side of a line that bisects the obtained circle in the cross-line direction. Figure 7c demonstrates the recorded SV-wave energy on the vertical component at given time and it follows the stationary behaviour with azimuth. At a given time the orientation of SV-wave polarization angle with respect to the vertical remains constant for each azimuth and ensures the stationary behaviour of the recorded energy on the vertical component.

REVO analysis of the recorded SH-wave energy on H_1 component indicates that a small amount of energy is registered on the H_1 component and is shown in Figure 8a. Figure 8b shows that SH-wave energy registration on H_2 component decreases with offset and polarity reversal occurs on the either side of zero offset. No energy is registered on the vertical component since SH-wave is decoupled from another seismic waves.

Time slices of the recorded SH wave energy on H_1, H_2 and the vertical components are shown in Figure 9a, b and c, respectively. Figure 8a reveals the variation of the recorded SH-wave energy on H_1 component with azimuth and demonstrates that energy registration decreases with azimuth and no energy is registered in cross-line direction. Energy registration on H_2 component increases with azimuth and no energy is registered in the in-line direction.

The zero offset travel time shown in Figures 5a, b, c and 8a, b, c indicates that SH- and SV- waves travel with same velocity along the symmetry axis. It is also noticed here that at large offset the arrival time of the SV- and SH- waves differs from each other. This phenomena is illustrated in more detail through the Figure 10. This figure shows the difference between the arrival time of the SV- and SH-wave at a geophone located at three different offsets' location, such as zero, medium and large offsets. If we ignore the dynamic behaviour of SH- and SV-waves and favourable component for the energy registration and are only concerned about travel time information, the observations from this figure are followed as:

- At zero offset both waves arrive at same time.
- At medium offset SV-wave energy is recognized by the geophone more than one time as supported by the cusps phenomena in anisotropic media.
- However, at far offset, the SH wave arrives prior to SV-wave

. These observations can be endorsed in the reference of the Figure 11. This figure reveals

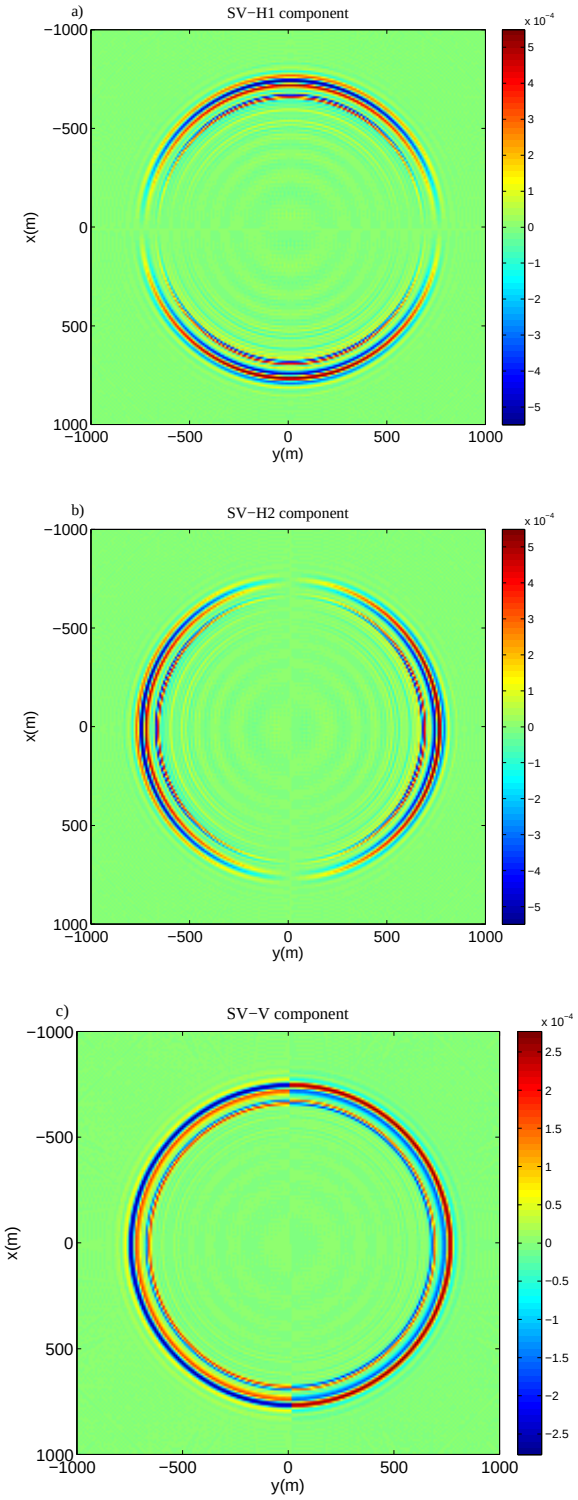

FIG. 7: (a) REVA of SV-wave on H_1 component and more than one concentric circle is the counter part of the triplication. Polarity reversal occur on the either side of a line that bisects the circle along in-line direction. (b) REVA analysis of SV energy on H_2 component demonstrate that H_2 component is more favourable for energy registration in the in-line direction. (c) REVA analysis of SV-wave on V component indicates that energy registration on V component follows the stationary behaviour. Polarity reversal occur on the either side of a line that bisects the circle along cross-line direction.

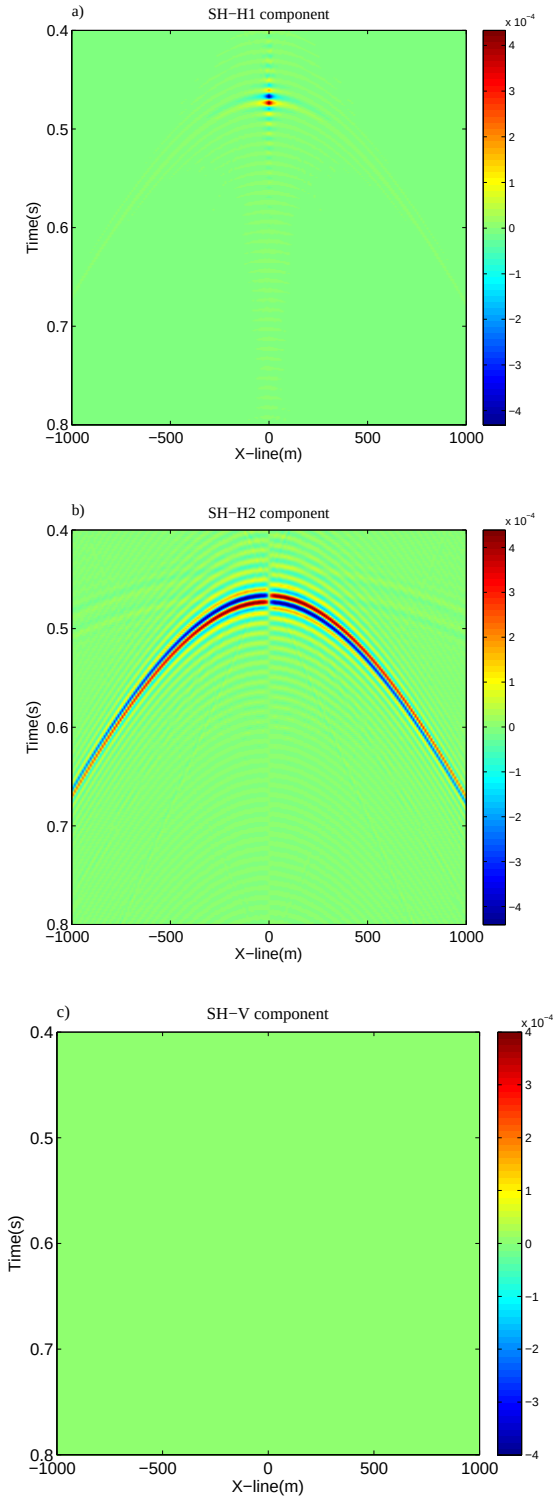

FIG. 8: (a) REVO analysis of SH-wave energy on H_1 component indicates that a small amount of energy is registered on H_1 component. (b) REVO of SH-wave energy on H_2 component. Energy registration decreases with offset and polarity reversal occur on either side of zero offset. (c) Recorded energy of SH-wave on Vertical component and it is null in this case.

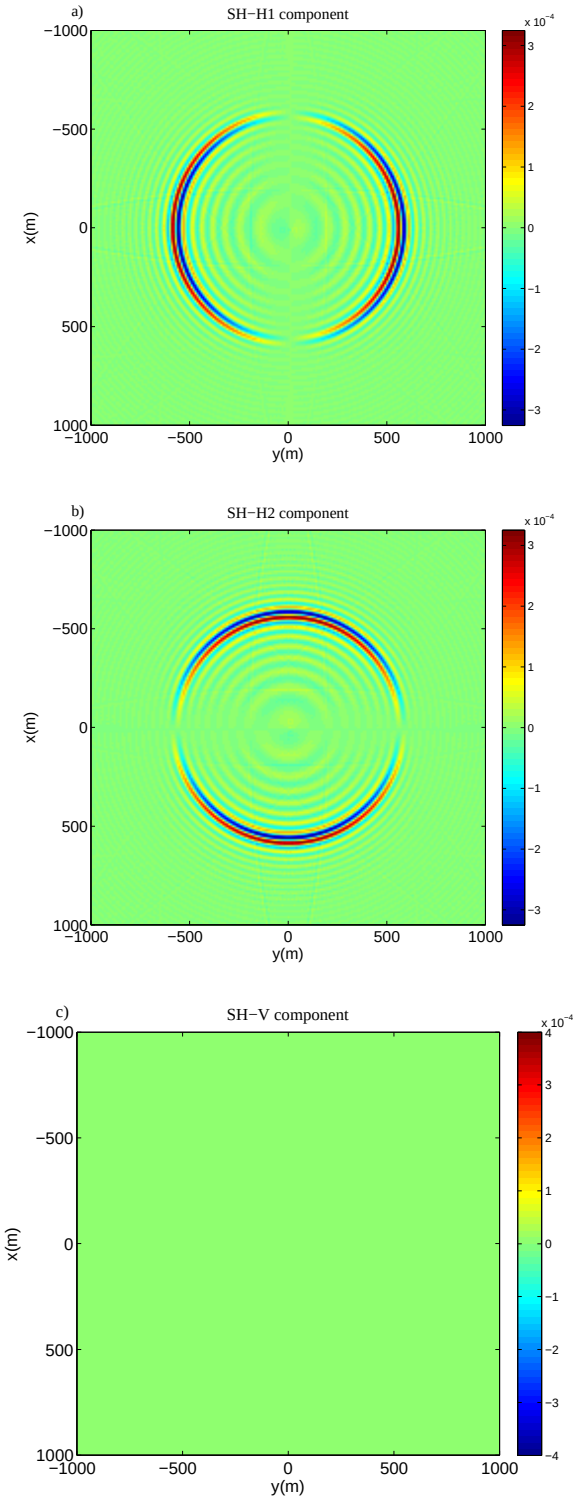

FIG. 9: (a) REVA analysis of SH-wave energy on H_1 component indicates that energy registration decreases as azimuth increases from 0 to 90. Polarity reversal occur on either side of a line that bisect the circle along cross-line direction. (b) REVA of SH-wave energy on H_2 component. Energy registration increases with azimuth and polarity reversal occur on either side of a line that bisect the circle along in-line direction . (c) Recorded energy of SH-wave on Vertical component and it is null in this case.

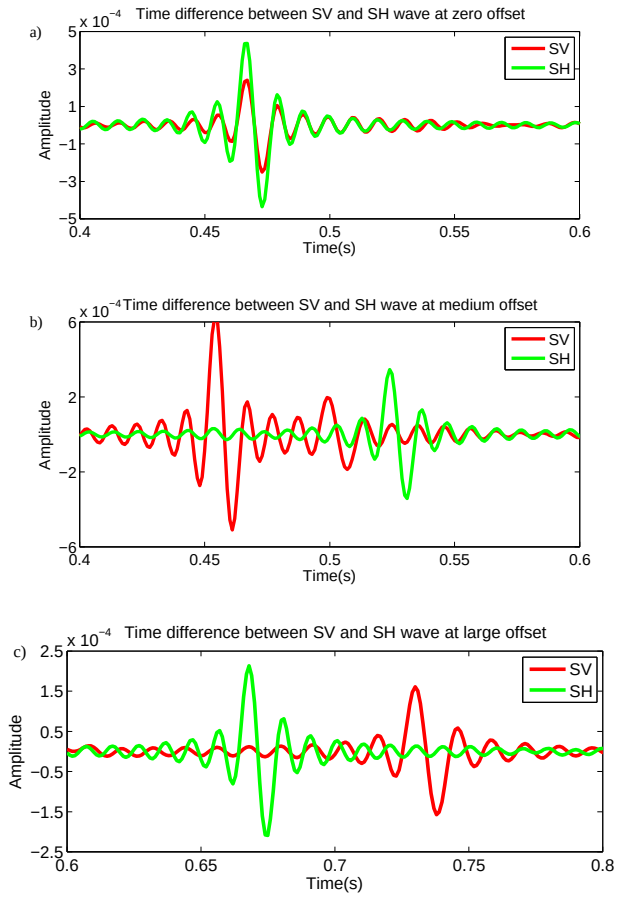

FIG. 10: The arrival time of the SV- and SH- waves at a geophone located at (a) zero offset (b) medium offset (c) far offset. At medium offset SV energy is arriving at two times (expected, unexpected). The unexpected arrival time of SV energy is supported by the cusps in anisotropic media. The arrival time of the SH-wave is less than that of SV-wave at far offset.

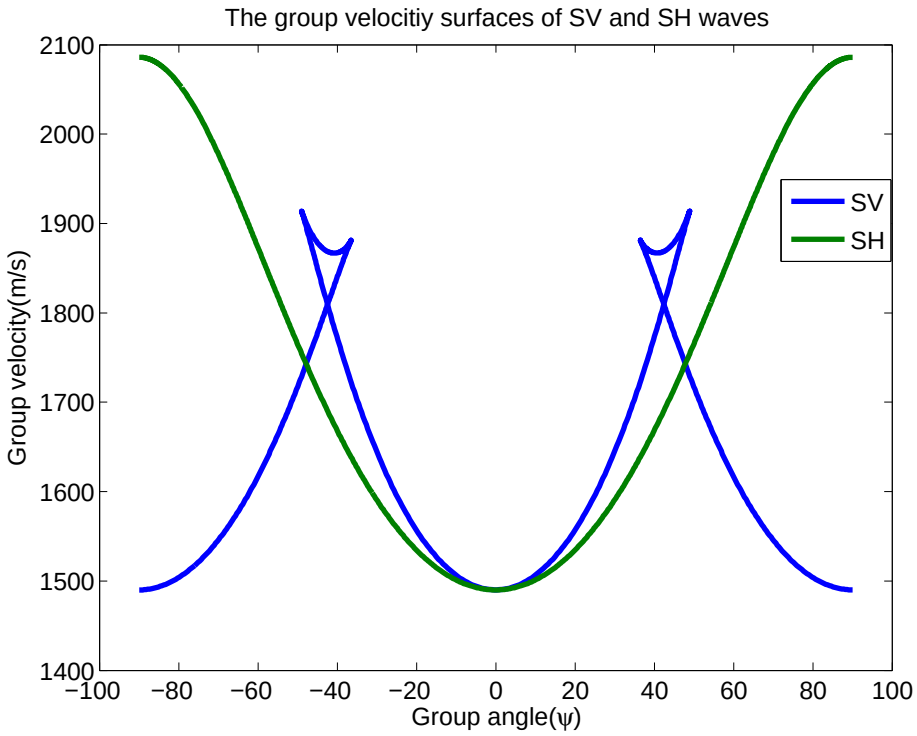

FIG. 11: The velocity variation of the SV- and SH-waves with the group angle. The velocity curve of the SV-wave shows the cusp phenomena and possesses multiple value at angle near by 45 degree in this case.

the group velocity behaviour with angle. It is observed that SH-wave velocity increases monotonically with angle(offset). Although, SV-wave velocity increases until maximum value is attained and then decreases and grasp the minimum value at far offset. As it is seen that up to medium offset, the SH-wave velocity surface lies below the SV-wave velocity surface, the arrival time of the SV-wave would be less than that of the SH-wave arrival time up to medium offset. At far offset, the SH-wave velocity surface attains its maximum value that is greater than the SV-wave velocity at the same offset and this behaviour shows the agreement for the occurred pattern of travel time of the SV- and SH-waves at far offset. It is also demonstrated that near by 45 degree of angle, the SV-wave velocity surface is multiple valued with cusp and reinforced to the occurred pattern of the unexpected arrival time of the SV-wave at medium offset.

CONCLUSION

$9C-3D$ seismic modelling for VTI has been accomplished in the plane wave domain. The authentication of the proposed extrapolation method has been demonstrated, kinematically. The REVO and REVA analysis of the known source (P, SV,and SH) on the components of the $3C$ geophone have been delineated here in order to illustrate favourable condition of energy registration on different components of the $3C$ geophone. Polarity reversal analysis with azimuth and offset has also been exposed. The phenomena of the triplication occurs in using an in-line source. This is supported by the another approach too.

REFERENCES

Aki, K., and Richards, P. G., 1980, Quantitative Seismology Theory and Methods: W.H.Freeman and Co.,San Francisco.

Ferguson, R. J., 2009, Geophone rotation analysis by polarity inversion: CREWES Research Report, **21**.

Ferguson, R. J., and Margrave, G. F., 2008, 3d phase shift operators: CREWES Research Report, **20**.

Ferguson, R. J., and Sen, M. K., 2004, Estimating the elastic parameters of anisotropic media using a joint inversion of p-wave and sv-wave travel time error.: Geophysical Prospecting.

Grechka, V., 2009, Application of Seismic Anisotropy in the Oil and Gas Industry.: EAGE.

Neufeld, C., and Clayton, C., 2000, Angle rotation in GLSB: Department of Civil and Environment Engineering-University of Alberta.

Sharma, R. K., and Ferguson, R. J., 2009, R and t coefficients for sh wave in plane wave domain: CREWES Research Report, **21**.

Slawinski, M. A., 2003, Seismic waves and Rays in Elastic Media.: Pergamon Second Edition.

Thomsen, L., 1986, Weak elastic anisotropy: Geophysics, **51**, No. 10, 1954–1966, discussion in GEO-53-04-0558-0560 with reply by author.

Tsvankin, I., 2001, Seismic Signatures and Analysis of Reflection data in Anisotropic Media.: Handbook of Geophysical Exploration Series.